ECCOMAS Congress 2016
VII European Congress on Computational Methods in Applied Sciences and Engineering
M. Papadrakakis, V. Papadopoulos, G. Stefanou, V. Plevris (eds.)
Crete Island, Greece, 5–10 June 2016

LAMINATE ELEMENT METHOD AND ITS APPLICATION TO THE STUDY OF GUIDED WAVE RESONANCE PHENOMENA IN LAYERED ELASTIC STRUCTURES WITH DEFECTS

Evgeny Glushkov[1], **Natalia Glushkova**[1], **Artem Eremin**[1], **and Rolf Lammering**[2]

[1]Institute for Mathematics, Mechanics and Informatics, Kuban State University
Krasnodar 350040, Russia
e-mail: evg@math.kubsu.ru

[2] Institute of Mechanics, Helmut-Schmidt-University/University of the Federal Armed Forces Hamburg
D-22043 Hamburg, Germany
e-mail: rolf.lammering@hsu-hh.de

Keywords: elastic guided waves; semi-analytical integral approach; laminate element method; resonance diffraction

Abstract. *A semi-analytical laminate element technique developed for the investigation of guided wave propagation and diffraction in layered structures with local inhomogeneities is presented. The approach is based on the use of fundamental solutions for the pristine layered structure as a basis functions for the scattered field approximation. As an example, its application to the investigation of resonance guided wave interaction with deep surface notches in elastic layer, which gradually change shape from rectangular to elliptical, has been considered to estimate the effect of notch geometry on resonance frequencies. The obtained numerical results are validated by the finite element simulation and experimentally confirmed on the basis of laser Doppler vibrometry.*

1 INTRODUCTION

Active structural health monitoring of plate-like units is commonly based on the propagation of elastic guided waves (GW) for long distances and their interaction with local inhomogeneities (defects) of various types [1]. The reflection, refraction and mode conversion phenomena serve as distinct indications of faults or defects. Computer simulation aims to clarify such a complex ultrasonic wave motion. General-purpose and specific finite-element computational codes have proven their efficiency for calculating wave propagation in elastic structures with complex geometry [2]. At the same time, with lengthy laminate waveguides, analytically based methods, such as boundary integral equation (BIE) technique and its derivations, e.g., boundary element method (BEM) or method of fundamental solutions (MFS), may serve as an efficient alternative [3]. They allow one to reduce the problem's dimension and obtain the results in a physically clear form of GW asymptotic expressions.

The laminate element method (LEM) [4] is a kind of boundary element technique specifically adjusted to simulate the elastodynamic behavior of lengthy layered structures. It is based on the boundary integral representations of elastic wave fields with the kernels in the form of fundamental solutions for the intact structure as a whole. Such basis functions called laminate elements (LEs) satisfy identically the governing equations in the sub-layers and interface boundary conditions among them as well as homogeneous conditions on the exterior plane-parallel surfaces. Therefore, only the integration over the obstacle's surface is necessary for the LE approximation of scattered wave fields.

In the current contribution, we present and discuss the LEM application to the investigation and parametric analysis of GW resonance phenomena in layered structures with obstacles. The resonance trapping mode effect [5] is featured by the capturing of incident wave energy and its prolonged localization in the defect's vicinity in the form of weakly decaying oscillations at the resonance frequencies [6]. The latter coincide with the spectral points of the corresponding boundary value problem (BVP) in the complex frequency plane. These frequencies strongly depend on the defect's size, shape and depth, making resonance effects a potentially useful tool for the enhancement and automation of the monitoring processes. In the calculations, they are approximated by the roots of the determinant of the linear algebraic system, to which the original BVP is reduced within the LEM approach.

A LEM based analysis of resonance wave phenomena is demonstrated on the examples of GW propagation and diffraction in aluminium specimens with surface notches of varying shape. The evaluated wave patterns and eigenfrequencies are compared with the results of FEM simulation and experimental data acquired using a contactless laser Doppler vibrometry allowing refined wave propagation sensing and visualization. The experimental and FEM-based results confirm the predicted values of resonance frequencies, revealing the trapping mode effect with a long standing-wave-type oscillation near the obstacles.

2 MATHEMATICAL MODEL

Let us consider a plane-strain time-harmonic oscillation $\mathbf{u}e^{-i\omega t},\ \mathbf{u} = \{u_x,\ u_z\}$, of a layered isotropic linear-elastic waveguide of thickness H governed by the Lamé equations. In the Cartesian coordinate system $\mathbf{x} = (x, z)$, the structure occupies the domain $D = \{|x| < \infty,\ -H < z < 0\}$ with surface and/or internal inhomogeneities (Fig. 1). The exterior plane-parallel surfaces $z = 0$ and $z = -H$ are stress-free except, possibly, at a local source zone Ω to which a load $\mathbf{q}_0$ is applied. Surface and internal defects are located to the right from this area, and their boundaries denoted by S are also traction-free.

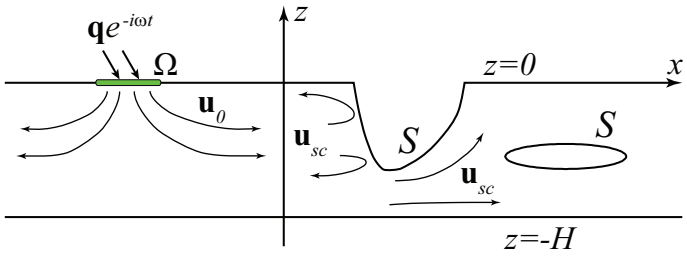

Figure 1: Schematic geometry of the problem.

The interaction of load-induced GWs $\mathbf{u}_0$ with obstacles results in the scattered field $\mathbf{u}_{sc}$. The total wave field $\mathbf{u}$ is a sum of the known, i.e., analytically expressed field $\mathbf{u}_0$ generated by the source in the pristine layer, and unknown scattered (reflected and transmitted) field $\mathbf{u}_{sc}$: $\mathbf{u} = \mathbf{u}_0 + \mathbf{u}_{sc}$.

Within the geometry considered, the incident field $\mathbf{u}_0(\mathbf{x})$ can be represented as a path integral of the inverse Fourier transform $\mathcal{F}_x^{-1}$ with respect to the horizontal coordinate x, which is further reduced to the far-field GW asymptotics using the residue technique:

$$\mathbf{u}_0(\mathbf{x}) = \tfrac{1}{2\pi}\int\limits_{\Gamma} K^+(\alpha,z)\mathbf{Q}_0(\alpha)e^{-i\alpha x}d\alpha \approx \sum_{m=1}^{M}\mathbf{a}_m(z)e^{i\zeta_m x}, \qquad (1)$$
$$\mathbf{a}_m(z) = -i\mathrm{res}K^+(\alpha,z)\mathbf{Q}_0(\alpha)|_{\alpha=-\zeta_m}$$

Here $K^+(\alpha,z) = \mathcal{F}_x[k^+(\mathbf{x})]$ and $\mathbf{Q}_0(\alpha) = \mathcal{F}_x[\mathbf{q}_0(\mathbf{x})]$ are Fourier symbols of the waveguide Green's matrix k^+ and load vector-function $\mathbf{q}_0$; the sign "+" indicates that the traction is applied to the upper surface $z = 0$; M is the number of real poles ζ_m of the Green's matrix $K^+(\alpha,z)$, the residues from which yield travelling waves. The sum in Eq. 1 is valid for the travelling GWs propagating to the right from the loading area Ω; the integration path Γ bypasses real poles ζ_m according to the principle of limiting absorption.

Within the indirect BIE formalism, the unknown field $\mathbf{u}_{sc}$ is sought for in terms of 2×2 LE matrix $l(\mathbf{x},\boldsymbol{\xi})$ integrated over the defect's boundary S together with an unknown source density $\mathbf{c}(\mathbf{x})$:

$$\mathbf{u}_{sc}(\mathbf{x}) = \int\limits_S l(\mathbf{x},\boldsymbol{\xi})\mathbf{c}(\boldsymbol{\xi})d\boldsymbol{\xi} \qquad (2)$$

In contrast to the classical fundamental-matrix solution $g(\mathbf{x}-\boldsymbol{\xi})$ for an infinite homogeneous elastic space [3], the matrix $l(\mathbf{x},\boldsymbol{\xi})$ is derived for the pristine infinite layered structure as a whole. Their columns $\mathbf{l}_j$ are displacement vectors $\mathbf{u}_j(\mathbf{x},\boldsymbol{\xi})$ associated with the point sources $\delta(\mathbf{x}-\boldsymbol{\xi})\mathbf{i}_j$ directed along the coordinate unit vectors $\mathbf{i}_1$ and $\mathbf{i}_3$ taken to be parallel to the axes x and z, respectively; $\boldsymbol{\xi} = (\xi_1,\xi_3)$ is the point of LE source location.

Being straightforward and computationally efficient, representation (1) inspires to derive the scattered field (2) in an analogous way. For this purpose the matrix $l(\mathbf{x},\boldsymbol{\xi})$ is constructed as a composition of the conventional fundamental solution matrix $g(\mathbf{x}-\boldsymbol{\xi})$ and non-singular matrix $v(\mathbf{x})$ that accounts for the fields reflected from the external sides of the structure and provides the required homogeneous boundary conditions at these plane-parallel boundaries: $l = g + v$. The matrix v, in its turn, is decomposed into two terms; each of them, being derived via the Green's matrices k^+ and k^- for the considered layer with non-zero stresses q^+ and q^- at the

upper and lower sufraces $z = 0$ and $z = -H$, respectively. With the tractions $q^{\pm}$ caused by the direct source field $g(\mathbf{x} - \boldsymbol{\xi})$, it takes the form::

$$v(\mathbf{x}) = \int_{\Gamma} [K^{+}(\alpha, z)Q^{+}(\alpha) + K^{-}(\alpha, z)Q^{-}(\alpha)]e^{-i\alpha x} d\alpha \tag{3}$$

where $Q^{\pm}(\alpha) = \mathcal{F}_x[-Tg(\mathbf{x} - \boldsymbol{\xi})]$ and T is the matrix of the stress operator for the external plane-parallel boundaries.

At the next step, the vector factor $\mathbf{c}(\boldsymbol{\xi})$ is discretized the same way as in the BEM, e.g., assuming a piecewise constant approximation over S. It gives rise to the following approximate representation for the scattered field:

$$\mathbf{u}_{sc} \approx \sum_{j=1}^{N} \mathbf{u}_{sc,j},\ \mathbf{u}_{sc,j}(\mathbf{x}) = \int_{S_j} l(\mathbf{x}, \boldsymbol{\xi})\mathbf{c}_j d\boldsymbol{\xi} = \mathbf{u}^{inf}_{sc,j}(\mathbf{x}) + \mathbf{u}^{c}_{sc,j}(\mathbf{x}) \tag{4}$$

$$\mathbf{u}^{inf}_{sc,j}(\mathbf{x}) = \int_{S_j} g(\mathbf{x} - \boldsymbol{\xi})\mathbf{c}_j d\boldsymbol{\xi}$$

Here S_j are segments of a polygon approximation of the smooth boundary S; $\mathbf{c}_j$ are 2×1 vectors of unknown constants. The non-singular component of the scattered field $\mathbf{u}^{c}_{sc,j}(\mathbf{x})$ can be represented in the way similar to expression (3):

$$\mathbf{u}^{c}_{sc,j}(\mathbf{x}) = \int_{\Gamma} [K^{+}(\alpha, z)\mathbf{Q}^{+}_{j}(\alpha) + K^{-}(\alpha, z)\mathbf{Q}^{-}_{j}(\alpha)]e^{-i\alpha x} d\alpha \tag{5}$$

$$\mathbf{Q}^{+}_{j} = \mathcal{F}_x[-T\mathbf{u}^{inf}_{sc,j}(x, 0)],\ \ \mathbf{Q}^{-}_{j} = \mathcal{F}_x[-T\mathbf{u}^{inf}_{sc,j}(x, -H)]$$

The derivation of scattered travelling waves is essentially based on the analytical evaluation of the vector-functions $\mathbf{Q}^{\pm}_{j}(\alpha)$. It is achieved using the trick, which is based on the specific rotation in the Fourier parameter space [7].

The unknown constants $\mathbf{c} = (\mathbf{c}_1, \mathbf{c}_2, ..., \mathbf{c}_N)$ are obtained from the system of linear algebraic equations $A\mathbf{c} = \mathbf{f}$, which arises from the substitution of relation (3) into the boundary conditions on S and further implementation of the Galerkin projection scheme. Resonance frequencies $\hat{\omega}_n$ of the considered BVP are approximated by the roots ω_n of the characteristic equation

$$\Delta(\omega) = \det A(\omega) = 0 \tag{6}$$

This equation is numerically solved using either Müller method (if a good initial guess of ω_n is known in advance) or with the argument principle approach.

3 RESULTS AND DISCUSSION

Recent theoretical and experimental investigations of the GW diffraction by deep rectangular notches in an elastic waveguide have revealed the trapping mode effect [8, 9]. Mathematically it is associated with the spectral points $\hat{\omega}_n = 2\pi\hat{f}_n$ of the BVP considered that are located in the complex frequency plane close to the real axis. While in a transient field this effect is featured by the wave energy localization near the obstacle, in the time-harmonic field it manifests itself in a strong resonance transmission of the incident wave at the frequencies $f_n \approx \mathrm{Re}\,\hat{f}_n$. Considering the pitting corrosion damage detection as a goal, it is of particular practical interest to further investigate such resonance phenomena for various notch shapes.

As an example, Fig. 2 demonstrates the A_0 mode transmission coefficient $\kappa^{+}(f)$ for various surface notches. Their shapes vary from the rectangle one (dashed curve No. 1, same as in Ref.

[8]) to the elliptical form (solid magenta curve No. 6). The coefficient κ^+ is introduced as the ratio of the time-averaged wave energy E_A^+ carried by the A_0 mode behind the obstacle to the incident wave energy E_0: $\kappa^+ = E_A^+/E_0$.

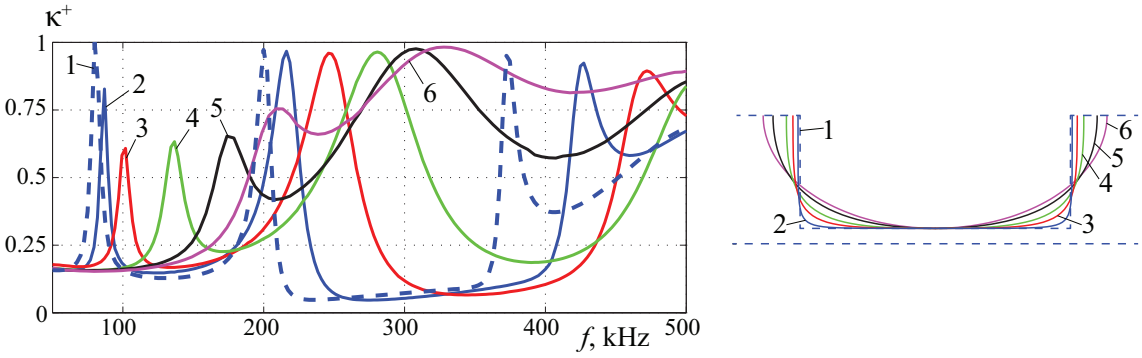

Figure 2: A_0 mode transmission coefficient κ^+ vs frequency f; curve 1: rectangular notch, 2: $p = 8$ in Eq. 7, 3: $p = 6$, 4: $p = 5$, 5: $p = 4$, 6: $p = 1$.

The input parameters for the calculations correspond to the aluminium plate samples used in the experiments: $Y = 70$ GPa, $\nu = 0.34$, $\rho = 2700$ kg/m^3; $H = 2$ mm; the initial obstacle is the surface sawed rectangular notch (width $a = 2$ mm, depth $d = 1.76$ mm), while the boundaries of other defects are constructed using the parametric equations

$$x = a_1 \cos^p(t), \quad y = b_1 \sin^p(t), \tag{7}$$

where $b_1 \equiv d$ and the parameter a_1 varies to provide the defect's square equal to $a \cdot d$; an elliptic surface occurs with $p = 1$.

It is clear from Fig. 2 that though the damage severity (its square and depth) remains the same, the defect's shape strongly influences on the peak transmission frequencies f_n. These frequencies f_n were taken as initial guesses for the $\hat{\omega}_n$ evaluation from Eq. 6. The first two complex eigenvalues of the considered BVP are summarized in Table 1 (in [kHz]).

Obstacle type	$\hat{f}_1$	$\hat{f}_2$	f_1^{FEM}	f_2^{FEM}
rectangular notch	81(1-i0.05)	200(1-i0.03)	81	216
$p = 8$	82(1-i0.04)	217(1-i0.05)	89	216
$p = 6$	97(1-i0.05)	246(1-i0.09)	115	255
$p = 5$	130(1-i0.06)	274(1-i0.14)	140	299
$p = 4$	182(1-i0.08)	306(1-i0.21)	181	316
elliptical notch	203(1-i0.11)	313(1-i0.27)	199	315

Table 1: The first two complex eigenvalues of the notched plates.

The validity of the obtained natural frequencies for a rectangular notch has been experimentally confirmed on the basis of laser Doppler vibrometry measurements with $f_1^{exp} = 85$ kHz and $f_2^{exp} = 215$ kHz [8]. However, the manufacturing of other notch types is not so straightforward and, therefore, FEM simulation with COMSOL Femlab 5.0 has been also used for the verification. For this purpose, following the strategy proposed in Ref. [10], eigenvalues of a finite

specimen, which is bounded by the defect's surface S from above and by the plane $z = -H$ from below with fixed side edges, are evaluated and summarized in the last two columns of Table 1, being in a considerable coincidence with the LEM-based results. At the same time, the FEM simulation does not account for the wave energy outflow to infinity. That is why it yields only real spectral points (resonance frequencies f_n^{FEM}) without imaginary parts that specify the damping rate of resonance oscillations.

Resonance GW interaction with defects is typically followed by a strong localization of oscillations in the vicinity of the obstacle. Examples of such localization are shown in Fig. 3, depicting spatial distributions of the amplitude $|u_z(x,z)|$ of the vertical displacement component at the frequencies $f_n \approx \mathrm{Re}\,\hat{f}_n$ for the rectangular and elliptical ($p = 1$) notches. The lower images are for the validating FEM results obtained for the aforementioned limited cuts from the specimens at the corresponding eigenfrequencies f_1^{FEM} and f_2^{FEM}. These eigenforms $u_z^{FEM}(x,z)$ are very close to the LEM-based obtained ones that are shown in the upper images. One can notice that in the case of elliptical notch the difference between the oscillation amplitudes inside and outside the defected region is not so contrast as for the rectangular obstacle due to the sufficiently bigger imaginary part in $\hat{f}_2$.

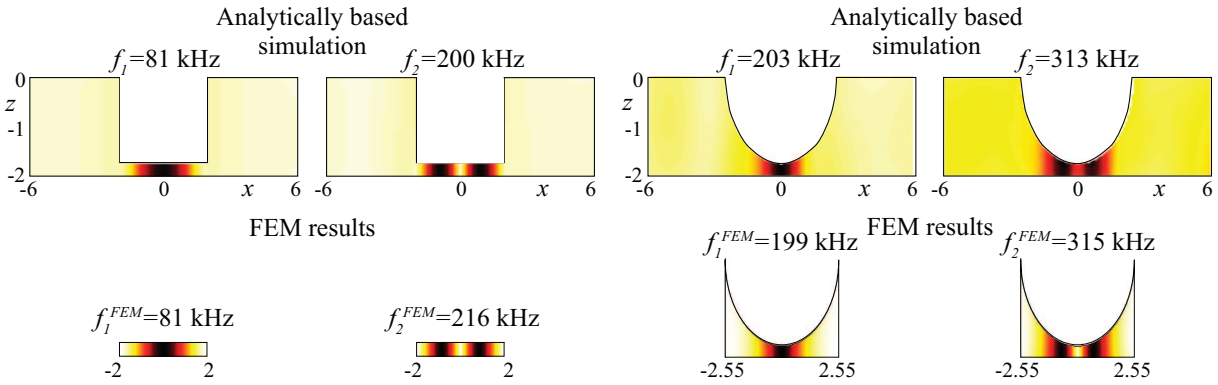

Figure 3: The patterns of resonance wave localization in the infinite waveguides (top plots) and corresponding eigenforms of the finite specimens (bottom plots) (dark regions correspond to higher amplitudes).

In the transient GW diffraction, natural frequencies $\hat{f}_n$ pronounce themselves with prolonged oscillations being localized at the obstacle region (trapping modes) [6]. The duration of such motion depends on the imaginary part of the corresponding eigenfrequency $\delta_n = 2\pi \mathrm{Im}\hat{f}_n$ through the factor $\exp(-\delta_n t)$. Though the real part of $\hat{f}_n$ is well approximated by FEM modelling, a LEM-based simulation for the infinite waveguide allows predicting both the resonance frequency and "quality" through the complete evaluation of complex $\hat{f}_n$.

In order to illustrate the influence of $\mathrm{Im}\hat{f}_n$ on the transient GW interaction with notches, the B-scans, which are out-of-plane surface velocity $v_z(x,t)$ along the x-axis depicted as functions of x and t, are shown in Fig. 4. The incident wave packets are generated by a remote surface-bonded piezoactuator excited with a Hann-modulated five-cycle bursts with central frequencies f_c close to the ones in the first and last rows of Table 1. As expected, in the case of rectangular defect, an intense and prolonged localization of wave energy at the notch is observed both theoretically and experimentally [8, 9]. At the same time, the growth of $\mathrm{Im}\hat{f}_n$ results in fast attenuation of oscillations in the defected area (two right images in Fig. 4). It is especially pronounced for the second eigenfrequency $\hat{f}_2$ of the elliptical notch. The motion at the obstacle vicinity stops just after the incident wavefield leaves this area.

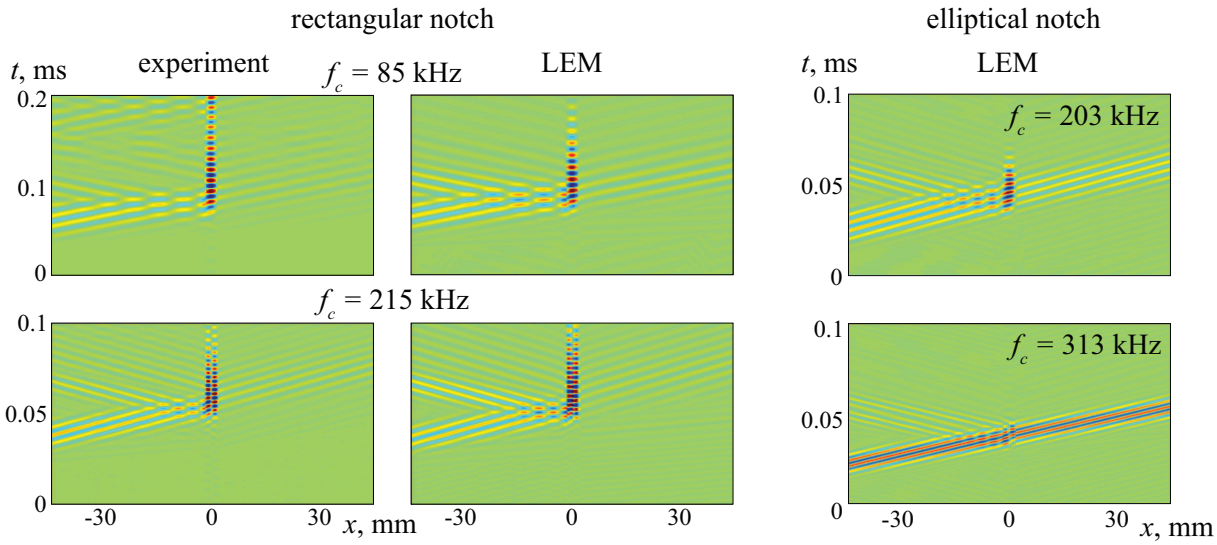

Figure 4: Localization of transient oscillations in the obstacle vicinity at the resonance frequency excitation that is ceased in the last case due to a high damping rate induced by comparatively large $\mathrm{Im}\hat{f}_n$.

4 CONCLUSIONS

A semi-analytical LEM-based approach is developed for the investigation of resonance diffraction of time-harmonic and transient GWs by a deep notch in a metallic plate. It allows revealing a strong dependence of the specimen's complex eigenfrequencies on the defect's shape and to study the influence of the eigenfrequency imaginary part on the intensity of the trapping mode effect.

The work is supported by the Russian Foundation for Basic Research (project No. 14-08-00370) and by the Russian Ministry of Science and Education (project No. 1.189.2014K).

REFERENCES

[1] T. Wandowski, P. Malinowski, W. Ostachowicz, M. Rawski, P. Tomaszewicz, T. Luba, G. Borowik, Embedded damage localization subsystem based on elastic wave propagation. *Computer-Aided Civil and Infrastructure Engineering*, **30**, 654–665, 2015.

[2] C. Willberg, S. Duczek, J.M. Vivar-Perez, Z.A.B. Ahmad, Simulation methods for guided wave-based structural health monitoring: a review. *Applied Mechanics Reviews*, **67**, 010803, 2015.

[3] M.H. Aliabadi, *The boundary element method. Volume 2: Applications in solids and structures*, John Willy & Sons LTD, 2002.

[4] Ye.V. Glushkov, N.V. Glushkova, A.A. Yeremin, V.V. Mikhas'kiv, The layered element method in the dynamic theory of elasticity. *Journal of Applied Mathematics and Mechanics*, **73**, 449-456, 2009.

[5] F. Ursell, Trapping modes in the theory of surface waves. *Mathematical Proceedings of the Cambridge Philosophical Society*, **47**, 347–358, 1951.

[6] E. Glushkov, N. Glushkova, M.V. Golub, J. Moll, C.-P. Fritzen, Wave energy trapping and localization in a plate with a delamination. *Smart Materials and Structures*, **21**, 125001, 2012.

[7] E. Glushkov, N. Glushkova, A. Ekhlakov, E. Shapar, An analytically based computer model for surface measurements in ultrasonic crack detection. *Wave Motion*, **43**, 458–473, 2006.

[8] E. Glushkov, N. Glushkova, A. Eremin, R. Lammering, Trapped mode effects in notched plate-like structures. *Journal of Sound and Vibration*, **358**, 142–151, 2015.

[9] E.V. Glushkov, N.V. Glushkova, A.A. Eremin, R. Lammering, Guided wave propagation and diffraction in plates with obstacles: resonance transmission and trapping mode effects. *Physics Procedia*, **70**, 447–450, 2015.

[10] I. Solodov, J. Bai, G. Busse, Resonant ultrasound spectroscopy of defects: Case study of flat-bottomed holes. *Journal of Applied Physics*, **113**, 223512, 2013.